Supporting Information

Jose Pinto,[‡†,] Andreas Weilhard,[‡*] Luke T. Norman,[‡] Rhys W. Lodge,[‡] David M. Rogers,[‡] Aitor Gual,[ᵟ] Israel Cano,[¥] Andrei N. Khlobystov,[‡] Peter Licence,[†*] and Jesum Alves Fernandes[‡*]

[‡]School of Chemistry, University of Nottingham, NG7 2RD, Nottingham, UK

[†]GSK Carbon Neutral Laboratories for Sustainable Chemistry, University of Nottingham, NG7 2TU, Nottingham, UK

[ᵟ]CTQC-Eurecat-UTQ, C/Marcel·lí Domingo 2, Building N5, 43007 Tarragona, Spain

[¥]Department of Inorganic Chemistry, Faculty of Chemistry, Universidad Complutense de Madrid, 28040 Madrid, Spain

*andreas.weilhard1@nottingham.ac.uk

*peter.licence@nottingham.ac.uk

* jesum.alvesfernandes@nottingham.ac.uk

1. General Information

All reagents were purchased from Sigma Aldrich and, if not stated elsewise, used without further purification. All solvents were of analytical grade, and all water used in this work was Millipore Milli-Q 18 MΩ ultrapure and deionised. Lithium bis(trifluoromethanesulfonyl)imide was acquired from IoLiTec GmbH. HCl (37 % v/V) and HNO_3 (69% v/V) are ARISTAR™' grade and purchased from VWR Chemicals. All solvents used for the catalytic experiments were of HPLC / GC grade. Research grade hydrogen (99.999%) was supplied by BOC – LINDE GROUP. All ILs investigated herein were prepared in our laboratory using modified literature procedures.[1, 2] All synthetized ILs were dried *in vacuo* (p ≤ 10^{-3} mbar) at 50 °C for 24 hours and stored under argon.

The synthesized materials contained no detectable impurities and chemical structure desired that were evaluated using ^{13}C and ^{1}H NMR, mass spectrometry, IR, Ion Chromatography and X-ray photoelectron spectroscopy (XPS). Nuclear magnetic resonance (NMR) measurements were performed at room temperature (RT) in a NMR Bruker Ascend™ 400 MHz Spectrometer; the chemical shift was referenced respect to tetramethylsilane (TMS at 0 ppm) and the solvent position ($CDCl_3$ at 7.24 ppm and 77.23 ppm, DMSO-d6 solvent at 2.5 ppm and 39.5 ppm for ^{1}H and ^{13}C NMR,

respectively). The coupling constants (J) are presented in Hz and the nomenclature used for the description of the multiplicity of the NMR signals is the following: singlet (s), doublet (d), double of doublets (dd), triplet (t), triplet of triplets (tt), sextet (sxt) and multiplet (m).

Mass spectroscopy measurements were carried out in a Bruker ESI-TOF MicroTOF II. Infrared spectroscopy (IR) was conducted using a Bruker Alpha (Fourier transform infrared) FTIR spectrometer with an ATR attachment. Ion Chromatography was used to evaluate the anion exchange and the presence of Chloride (Cl^-) from IL precursor using a Dionex ICS-3000 fitted with AS20 analytical column and AG20 guard column. UV-vis absorbance spectroscopy was measured using a Cary 5000 UV-vis spectrophotometer (Agilent), equipped with a UV-Vis Internal Diffuse Reflectance sphere (Internal DRA-2500 PMT/PbS) using quartz cuvettes with a 1 mm path length. All ILs were then stored in a glove-box along with all metal-containing samples. TEM measurements were always (if not stated otherwise) carried out at the Nanoscale and Microscale Research Centre (NMRC) in a JEOL 2100F FEG-TEM with Oxford Instruments ISIS EDS analysis system operating at 200 kV. ICP-OES measurements were undertaken on a Perkin Elmer Optima 2000 DV Inductively Coupled Plasma Optical Emission Spectrometer. GC-FID analysis were performed in a Thermo Trace 1310 using He (constant flow of 20 mL min^{-1}) gas as the carrier with the TG17MS column (30 m × 0.25 mm × 0.25 μm). XPS measurements were performed using a Kratos AXIS Ultra spectrometer instrument with a focused monochromated Al Kα source (hv = 1486.6 eV) equipped with hybrid magnetic lens (magnetic/electrostactic), concentric hemispheriscal analyser (CHA), and a multi-channel plate and delay line detector (DLD).

2. Synthesis and characterisation of ionic liquids (IL)
1-Butyl-3-methylimidazolium Chloride, [C$_4$C$_1$Im]Cl[1]

To a solution of 1-methylimidazole (10.2 ml, 128.4 mmol) in acetonitrile (25 mL), 1-chlorobutane (16.0 mL, 153.9 mmol) was added dropwise whilst stirring (600 RPM) at RT. The reaction mixture was heated at 40 °C in a round neck bottomed flask fitted with a reflux condenser under continuous stirring (600 RPM) for 48 h. A biphasic mixture was formed with the top layer containing unreacted material, which was decanted. Ethyl acetate was added (50 mL) with comprehensive mixing and left to settle before being decanted. This procedure was repeated twice to eliminate

unreacted material. The crude solid was recrystallized twice using a mixture of acetonitrile/ethyl acetate. The supernatant solvent was decanted and the obtained product was dried *in vacuo* (at 7.0 x 10^{-4} mbar) using an intermediate secondary trap (first 8 hours) at 50 °C for 48 h to yield a white hygroscopic solid (16.19 g, 72.2%) with a melting point of 70 °C.

^{1}H NMR (400 MHz, DMSO-d_6) δ (ppm): 0.89 (t, *J* = 7.4 Hz, 3 H), 1.26 (sxt, *J* = 7.4 Hz, 2 H), 1.77 (tt, *J* = 7.4 Hz, 2 H), 3.85 (s, 3 H), 4.17 (t, *J* = 7.4 Hz, 2 H), 7.65 (t, *J* = 1.8 Hz, 1 H), 7.75 (t, *J* = 1.8 Hz, 1 H) and 9.10 (s, 1 H).

^{13}C NMR (100 MHz, DMSO-d_6) δ (ppm): 13.2, 18.7, 31.3, 35.7, 48.5, 122.2, 123.6, 136.5.

IR, *v* (cm^{-1}): Bending (O-H): 1640 cm^{-1}; Stretching (O-H): 3450 cm^{-1}, Stretching (C-H): 3000-3100 cm^{-1}; Bending (C-H): 1350-1480 cm^{-1}; Stretching (C-H): 2850-3000 cm^{-1}; Stretching (C=N): 1080-1360 cm^{-1}; Stretching (C=C): 1400-1600 cm^{-1}.

ESI-MS (+ve) $[C_8H_{15}N_2]^+$ calcd: 139.1232; found: 139.1245
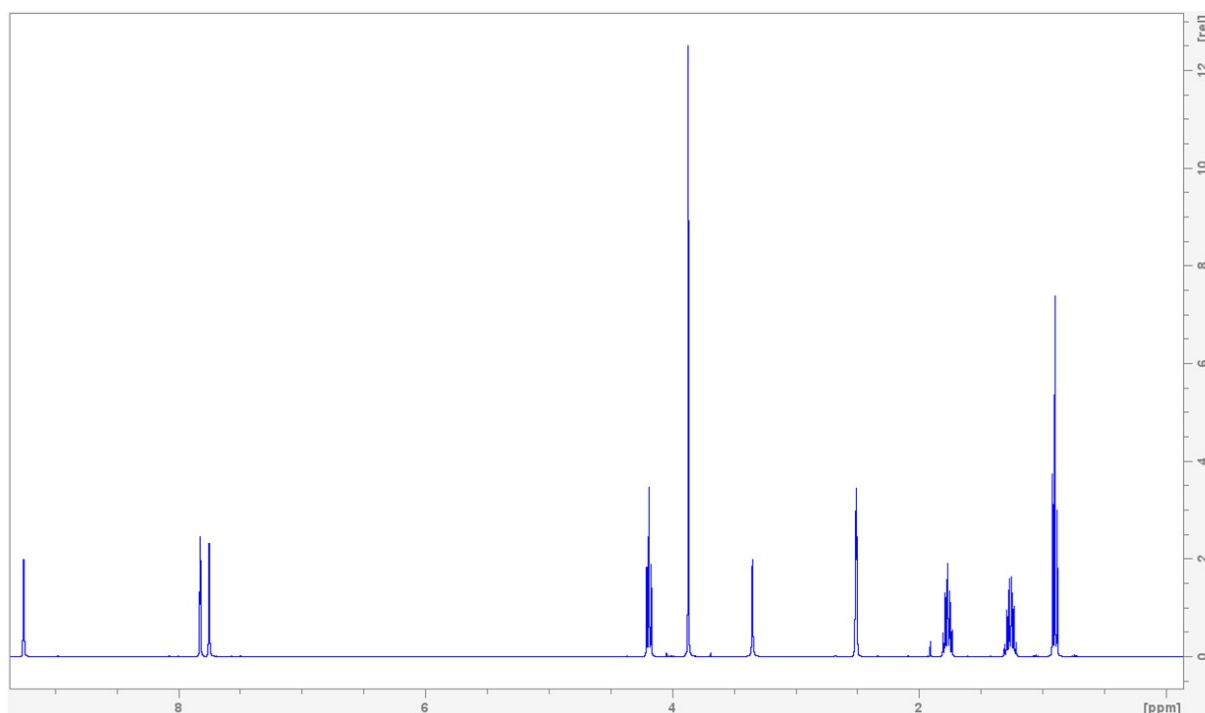
Figure S1. ^{1}H-NMR of C_4C_1Im.Cl in dmso-d_6.

<u>1-Butyl-3-methylimidazolium bis(trifluoromethanesulfonyl)imide, [C$_4$C$_1$Im][NTf$_2$][1, 2]</u>

To a stirred (600 RPM) solution of [C$_4$C$_1$Im]Cl (10 g, 57.2 mmol) in ultrapure water (70 ml), a solution of Lithium bis(trifluoromethane)sulfonimide (1.1 eq, 18.1 g, 62.9 mmol) in ultrapure water (50 mL) was added dropwise, at RT. The resulting reaction mixture was stirred for 24 hours at RT. Dichloromethane (100 ml) was added and the organic layer extracted by liquid/liquid separation and washed with ultrapure water (4 x 20 mL) to remove unreacted material. The solvent was removed under *vacuo* (7.0 x 10^{-4} mbar) at 50 °C for 48 h using an intermediate secondary trap yielding a colourless liquid (45.5 g, 94.6%).

^{1}H NMR (400 MHz, DMSO-d$_6$) δ (ppm): 0.90 (t, *J* = 7.4 Hz, 3 H), 1.26 (sxt, *J* = 7.4 Hz, 2 H), 1.77 (tt, *J* = 7.4 Hz, 2 H), 3.85 (s, 3 H), 4.16 (t, *J* = 7.4 Hz, 2 H), 7.68 (t, *J* = 1.8 Hz, 1 H), 7.75 (t, *J* = 1.8 Hz, 1 H), 9.10 (s, 1 H).

^{13}C NMR (100 MHz, DMSO-d$_6$) δ (ppm): 13.2, 18.7, 31.3, 35.7, 48.5, 119.9 (q, J = 322 Hz, -CF$_3$), 122.2, 123.6, 136.5.

^{19}F NMR (377 MHz, DMSO-d$_6$) ([C$_4$C$_1$Im] [NTf$_2$]) - δ (ppm): -78.8 (s, 6 F).

IR, *v* (cm^{-1}): Stretching (C-H): 3000-3100 cm^{-1}; Bending (C-H): 1350-1480 cm^{-1}; Stretching (C-H): 2850-3000 cm^{-1}; Stretching (C=N): 1080-1360 cm^{-1}; Stretching (C=C): 1400-1600 cm^{-1}; Stretching (S=O): 1060 cm^{-1}; Stretching (C-F): 1200 cm^{-1}.

ESI-MS (+ve) [C$_8$H$_{15}$N$_2$]$^+$ calcd: 139.1232; found: 139.1245

ESI-MS (-ve) [C$_2$F$_6$NO$_4$S$_2$]$^-$ calcd: 279.9173; found: 279.9180

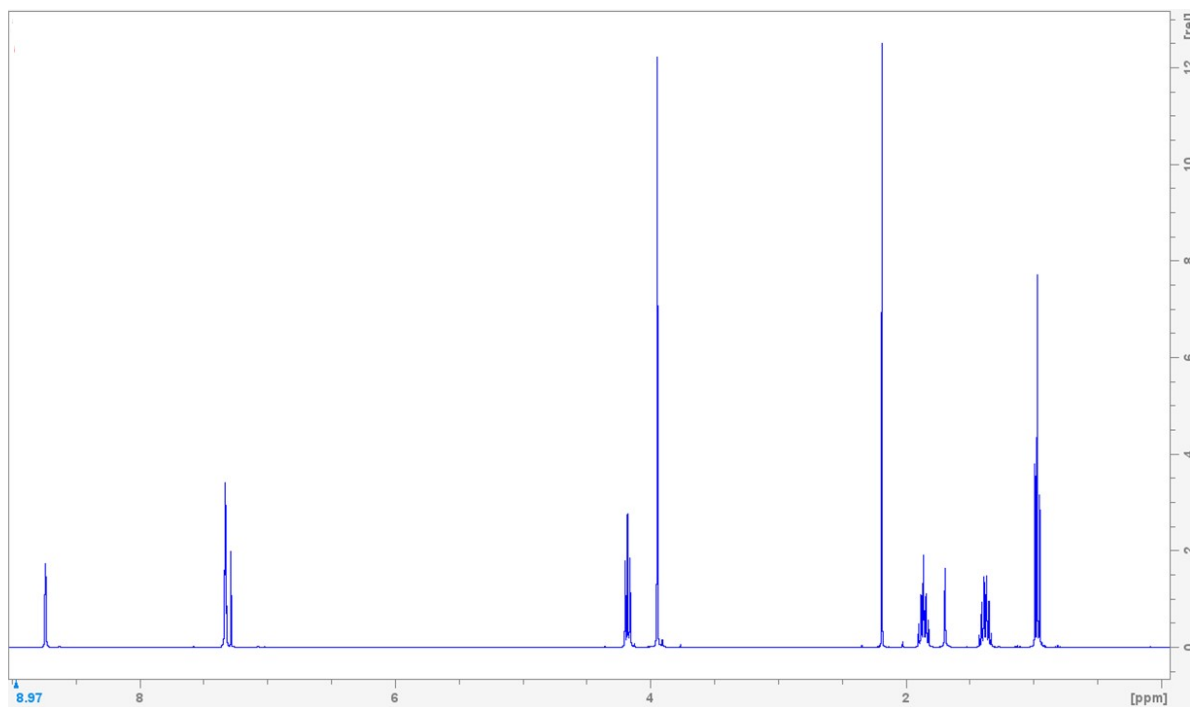**Karl Fischer Titration:** 8.5 ppm of water.

Ion Chromatography: < 1% Chloride.

Figure S2. ^{1}H-NMR of $C_4C_1Im.NTf_2$ in dmso-d$_6$.

3. Synthesis and general characterization of Pd, Au and PdAu nanoparticles (NPs)

Pd, Au and PdAu NPs were produced using a bespoke AJA magnetron sputtering system with a load-lock sample transfer facility coupled to a glove-box. The Pd and Au targets (99.995 %) were purchased from AJA International. IL samples were loaded through a glove-box into the magnetron sputtering system to avoid the presence of moisture (**Figure S3**).
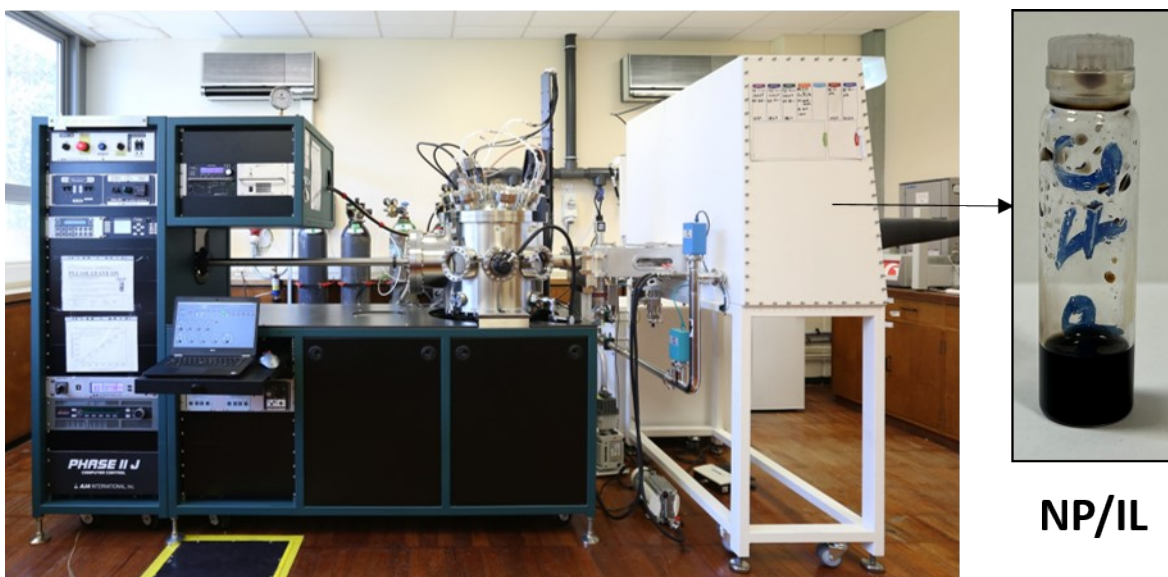
NP/IL

Figure S3. Photo of the magnetron sputtering system located at the School of Chemistry – University of Nottingham used in this work; and an inset of the NP/IL after metal species deposition in ionic liquid.

In a typical experiment, anhydrous [C_4C_1Im][NTf_2] (0.750 g) is placed into a petri dish in the glove box. The sample was transferred to a load-lock under a N_2 environment, pumped-down to a background pressure of 5×10^{-5} Pa for *ca.* 1 h and then transferred to the main chamber, which reached a background pressure of 5×10^{-6} Pa for *ca.* 1 h (**Figure S3**). Pd, Au and PdAu NPs were prepared in [C_4C_1Im][NTf_2] by magnetron sputtering process. PdAu NPs were synthesized using co-deposition mode, where Pd and Au targets were sputtered at the same time. The composition of the samples was adjusted by the use of different powers applied as can be seen in **Figure S4** and Table S1. The working pressure employed in all depositions was 4.0×10^{-1} Pa (Argon - 99.9999 %). The other parameters used during depositions are described in Table S1. After all depositions were carried out, the samples were kept under inert atmosphere in the glove-box.

The resulting composition of the PdAu NPs were analysed by ICP-OES. 20 mg of a sample was accurately weighted in a flask, per each sample, in triplicate (3 X 20 mg). 300 mg of a solution of one part concentrated nitric acid and three parts concentrated hydrochloric acid (aqua regia) was added to each flask. After 24 h, the metals were completely dissolved in the solution. Afterwards, the obtained solutions were diluted and transferred into a 10 ml volumetric flask using a 5% HCl solution (% v/v in ultrapure water). The volumetric flasks were filled to the mark with this 5% HCl solution, and then analysed using calibration curves with the appropriate calibration standards.

6

Each sample was measured in 2 different wavelengths, with high sensitivity for each element. Wavelengths used for the determination of gold content in solution were 267.595 nm and 242.795 nm, and for palladium 340.458 nm and 363.470 nm. The obtained values for the triplicates were averaged, and then the error was determined using the standard deviation of the obtained measurements.
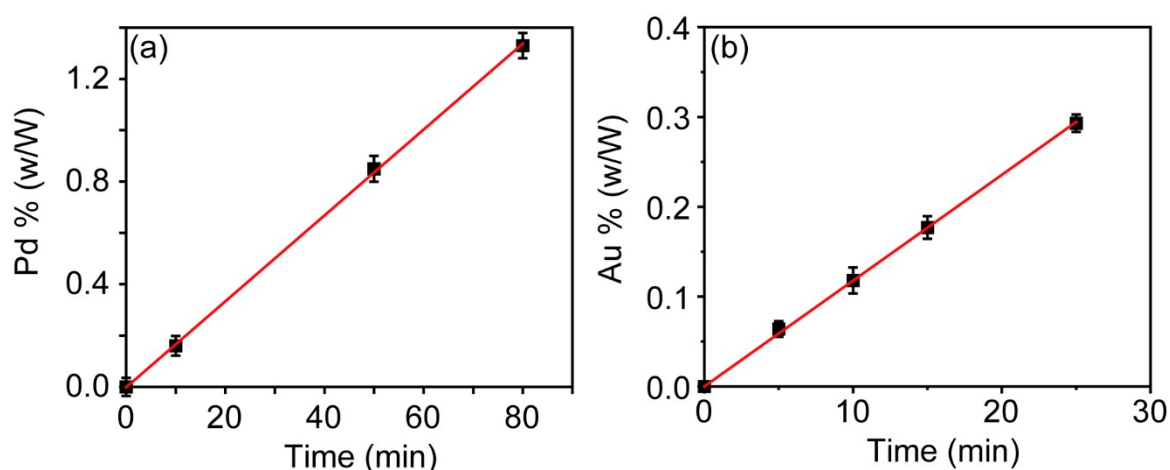

Figure S4. Calibration experiments to adjust the PdAu NPs composition. (a) Pd deposition in IL using 60 W, which generates a deposition rate of 0.016% Pd(w/w) min^{-1}. (b) Au deposition in IL using 60 W, which generates a deposition rate of 0.015% Au(w/w) min^{-1}.

Table S1. Summary of magnetron sputtering parameters using co-deposition mode for the production of Pd, Au and Pd Au NPs in [C_4C_1Im][NTf_2].

Sample	Deposition time (min)	Power applied (W)		Metal via ICP-OES (at%)(wt%)		Metal via XPS (at%)
		Pd	Au	Pd	Au	Pd
Pd	50.0	60.0	-	(100)(0.85)	-	-
Pd$_{0.75}$Au$_{0.25}$	50.0	60.0	15.0	(75.3)(0.87)	(24.7)(0.53)	(76.2)
Pd$_{0.50}$Au$_{0.50}$	50.0	60.0	90.0	(52.4)(0.85)	(47.6)(1.43)	(53.1)
Pd$_{0.25}$Au$_{0.75}$	180	30.0	120	(18.7)(0.85)	(81.3)(6.82)	(20.2)
Au	50.0	-	30.0	-	(100)(0.85)	-

TEM measurements

Transmission electron microscopy (TEM) measurements were performed using a JEOL 2100F FEG-TEM operated with an accelerating voltage of 200 kV. TEM samples were prepared on copper mesh, holey carbon film TEM grids (Agar Scientific, UK) with Ar glow discharged (Agar Turbo Coater, 0.2 mbar, 5 mA, 10 secs) before the addition

of NPs@IL (10 µL). The NPs@IL suspension was kept on the grid for 2 minutes before the excess was removed using filter paper. The size distribution histogram (below each TEM image) was obtained by counting 300 NPs from a minimum of 7 images for each sample.
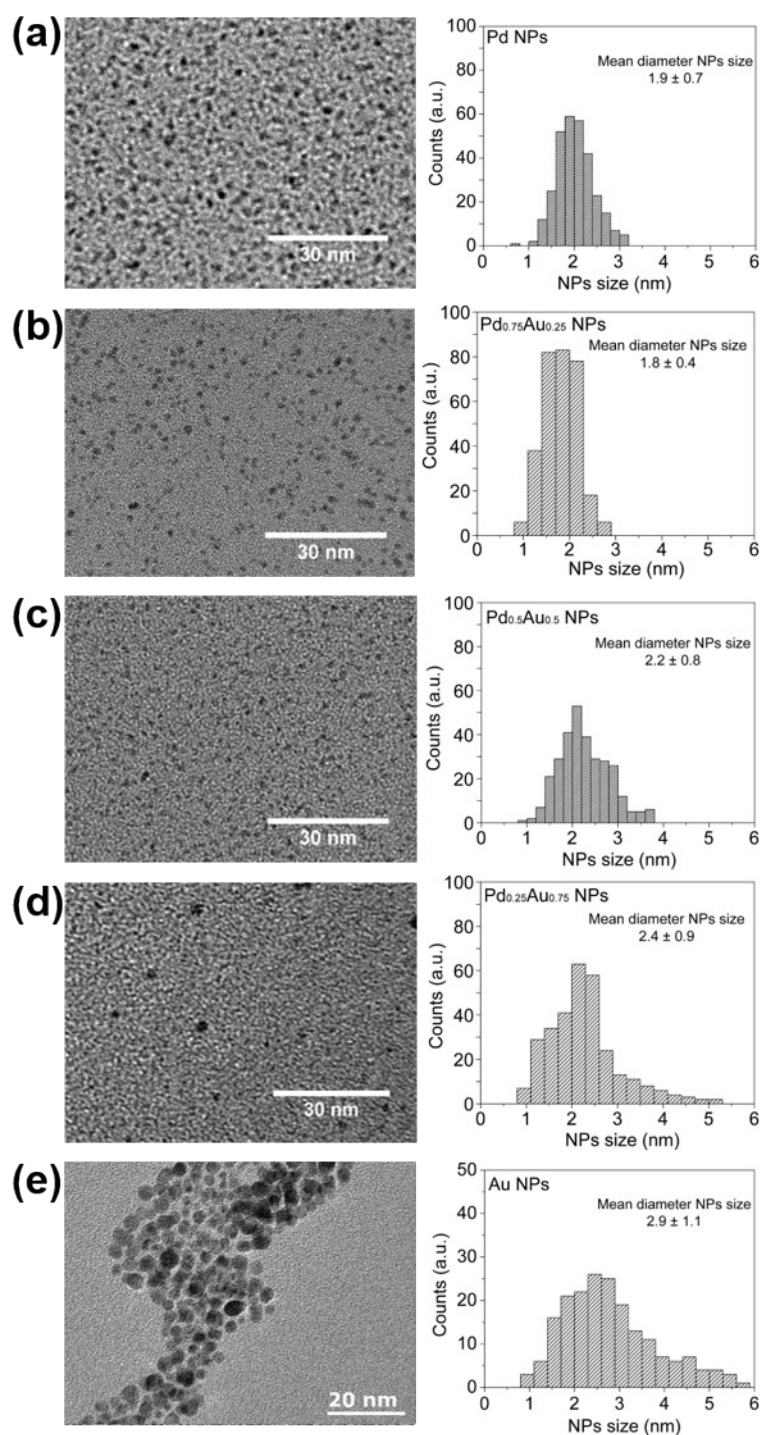

Figure S5. TEM images and size distributions histograms of Pd, Au and PdAu NPs in [C_4C_1Im][NTf_2]. **(a)** Pd NPs, **(b)** $Pd_{0.75}Au_{0.25}$ NPs, **(c)** $Pd_{0.5}Au_{0.5}$ NPs, **(d)** $Pd_{0.25}Au_{0.75}$ NPs, and **(f)** Au NPs.

XPS measurements

XPS measurements were performed using a Kratos AXIS Ultra DLD instrument. The chamber pressure during the measurements was 6.7×10^{-7} Pa. Wide energy range survey scans were collected at pass energy of 80 eV in hybrid slot lens mode and a step size of 0.5 eV, for 20 min. High-resolution data on the Pd 3d, Au 4f C 1s, N 1s, O 1s, S 2p and F 1s photoelectron peaks were collected at a pass energy of 20 eV over energy ranges suitable for each peak, and collection times of 5 min, step sizes of 0.1 eV. The charge neutralizer filament was used to prevent the sample charging over the irradiated area. The X-ray source was a monochromated Al Kα emission, run at 10 mA and 12 kV (120 W). The energy range for each 'pass energy' (resolution) was calibrated using the Kratos Cu $2p_{3/2}$, Ag $3d_{5/2}$ and Au $4f_{7/2}$ three-point calibration method. The transmission function was calibrated using a clean gold sample method for all lens modes and the Kratos transmission generator software within Vision II. The data were processed with CASAXPS (Version 2.3.17). The high-resolution data was charge corrected to the reference F 1s signal at 688.9 eV, as no peak deconvolution is required increasing the reliability of the charge reference. After that, all the other peaks positions for S 2p, N 1s, C 1s and O1s were calibrated against the F 1s peak, showing good agreement with previous reports in the literature.[3, 4]

Samples were prepared by placing a small drop (<10 mg) of ionic liquid into a standard stainless steel multi-sample bar (Kratos design) inside a glove box; and then the multi-sample bar was placed into a sealed box. The sealed box was carried to the next room where the XPS instrument is located, and then introduced into the instrument immediately after preparation to avoid absorption of moisture.
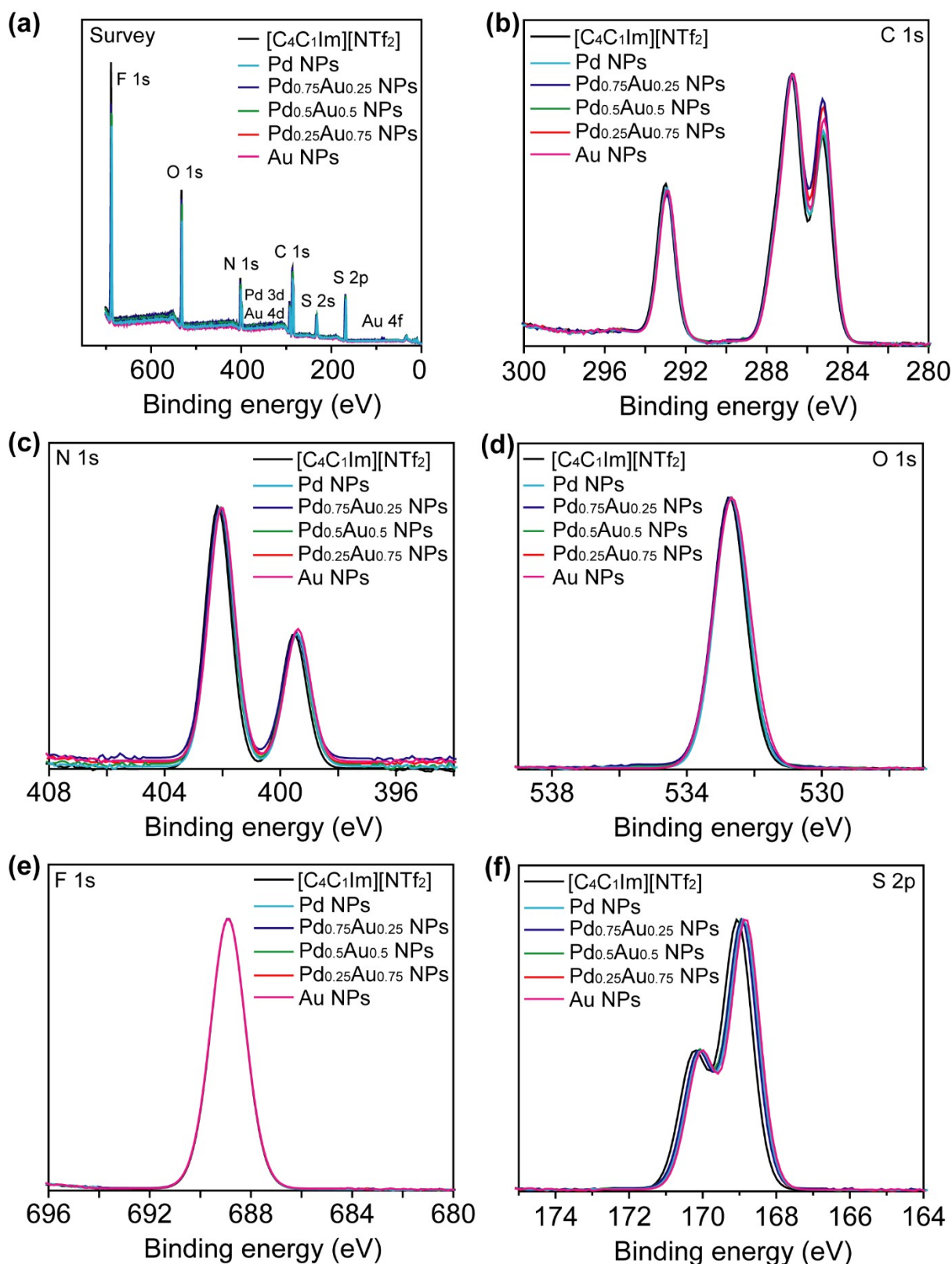
Figure S6. XPS spectra of [C$_4$C$_1$Im][NTf$_2$], and Pd, Au and PdAu NPs in [C$_4$C$_1$Im][NTf$_2$]. **(a)** Wide scan, **(b)** C 1s, **(c)** N 1s, **(d)** O 1s, **(e)** F 1s and **(f)** S 2p. No significantly difference in the XPS spectra were observed in the IL after the metal species deposition.[4]

X-ray Absorption Spectroscopy (XAS)

X-ray absorption (XAS) measurements were performed at RT at the Pd K-edge and Au L_3-edge in the B18 beamline at the Diamond Synchrotron Light and Balder line in MAX-IV. X-ray absorption near edge structure (XANES) and extended X-ray absorption fine structure (EXAFS) spectra of a Pd and Au foil standards were measured and the energy calibrated by aligning the respective absorption edges. The data were calibrated and normalized by a linear pre-edge subtraction using ATHENA software.[4-6]

The metal catalysts in IL were placed into a glass vials (see inset in **Figure S3**) inside a glove box after the deposition, and then placed in a sealed box that was used to transport the samples to the Diamond Light Source and MAX-IV synchrotron. XANES and EXAFS measurements were carried out using the glass vials as sample holder, thus the NPs/IL were not exposed directly to moisture during the measurements.

4. Catalytic Experiments

General information

The catalytic tests were performed in an in-house built Fisher-Porter reactor system. The system is equipped with a sampling loop of 0.1 mL enabling the collection of reaction aliquots over time without depressurizing the reactor. The Fisher-Porter reactor system has a maximum volume of 22 mL and was rated to a maximum pressure of 22 bar.

Typical catalytic experiment

The desired amount of cinnamaldehyde (CAL), dihydrocinnamaldehyde (HCAL), tridecane (200 µL, 151 mg, 8.2 mmol) and NPs@IL (130 mg, Pd concentration = 0.5 mM) were dissolved in THF (10 mL) and heated to 50°C. The reactor was flushed 3 times with H_2 to exchange the atmosphere and finally pressurized to the desired pressure with H_2. The reaction was vigorously stirred at 600 RPM and sampled frequently to monitor the reaction progress. Aliquots were diluted in THF and the concentrations were determined using a GC-FID using tridecane as an internal standard.

<u>Delay experiment</u>

In a typical delay experiment NPs@IL (130 mg, Pd concentration = 0.5 mM) and tridecane (200 µL, 151 mg, 8.2 mmol) are dissolved in THF (10 mL) and stirred at 50°C for the time τ under a N_2 atmosphere. Then, CAL is added and the reactor flushed 3 times with H_2 to remove N_2 and then pressurized to 5 bar and stirred at 50°C. Aliquots are taken during the reaction as described previously to determine the reaction progress. Concentrations are determined using a GC-FID and tridecane is used as an internal standard. The effect of individual reagents and product(s) are determined by adding these to the reaction mixture for the time τ. The effect of CAL was determined by adding CAL (629 µL, 661 mg, 5 mmol). The effect of HCAL was determined by adding HCAL (664 µL, 671 mg, 5 mmol). The effect of H_2 was determined by pressurizing the reactor to 5 bar. In the case of H_2: After the time τ the reactor was vented and CAL (629 µL, 661 mg, 5 mmol) was added and the reactor was pressured.
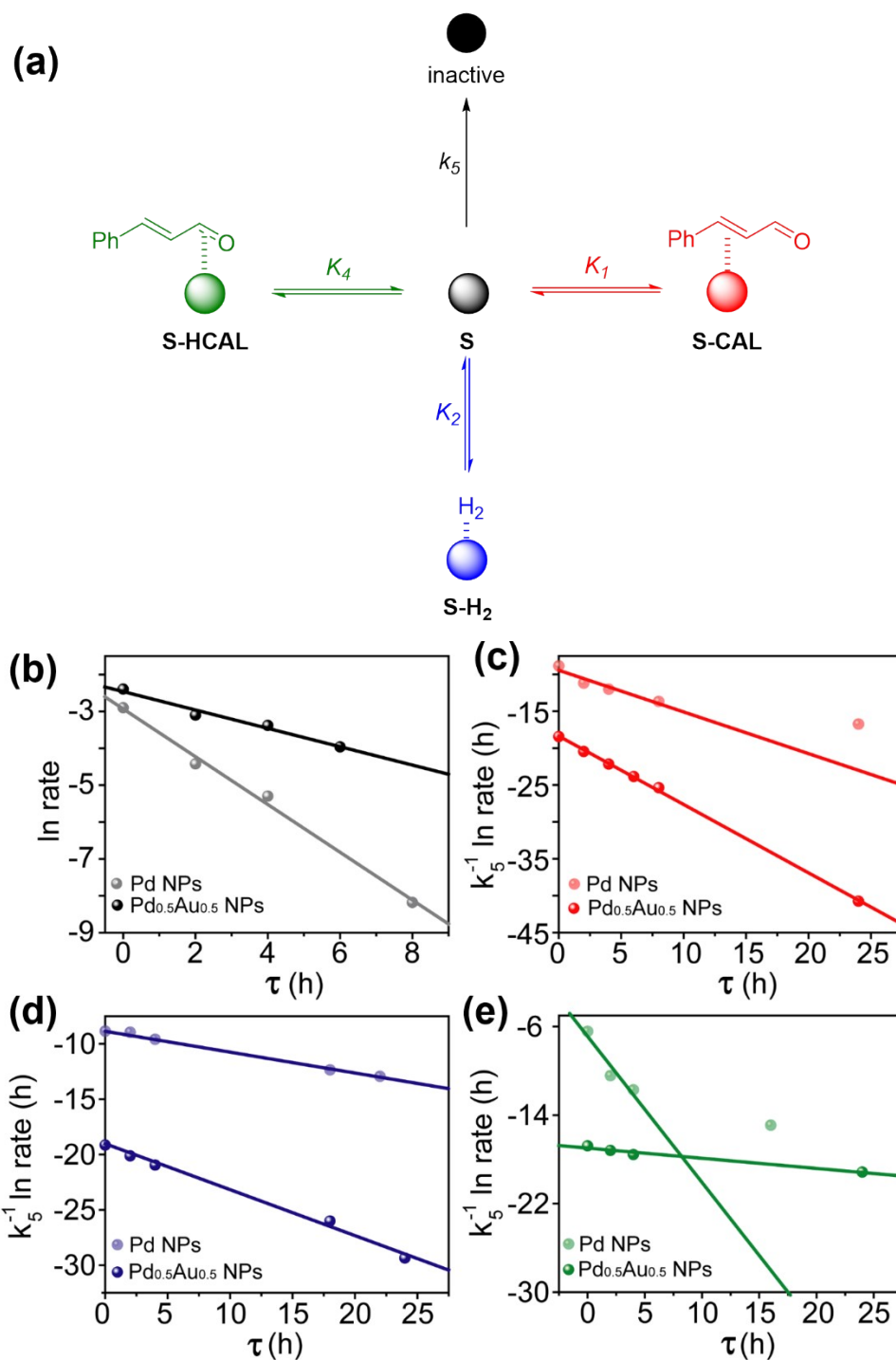
Figure S7. (**a**) The various resting states of the applied Pd and $Pd_{0.5}Au_{0.5}$ NPs (highlighted in red, blue and green), and the formation of an inactive site. (**b**) Reduction of the initial rate, plotted on a logarithmic scale, suggested a first order rate dependency for catalyst deactivation upon a pre-incubation period τ, $k_{5, Pd} = 0.33$ h^{-1} and $k_{5, Pd0.5Au0.5} = 0.13$ h^{-1}. (**c-e**) Reduction of the initial catalytic rate upon subjection to a pre-incubation period τ in the presence of 0.5 M CAL (**c**), 5 bar H_2 (**d**) and 0.5 M HCAL (**e**). Reaction conditions (**b**) - (**e**): THF (10 mL), T = 50°C, $P(H_2) = 5$ bar, [CAL] = 0.5 M, Pd concentration for both $Pd_{0.5}Au_{0.5}$ and Pd as catalyst was 0.5 mM and (**e**) THF (10 mL), T = 50°C, $P(H_2) = 5$ bar, [HCAL]=[CAL] = 0.5 M, Pd concentration for both $Pd_{0.5}Au_{0.5}$ and Pd as catalyst was 0.5 mM.
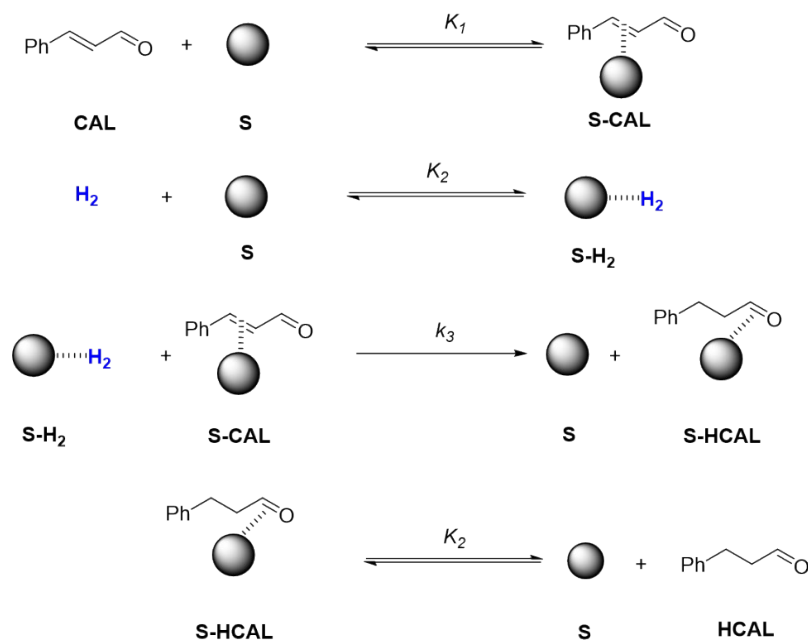
Deriving rate laws

The loss of catalytically active sites was derived as shown below.
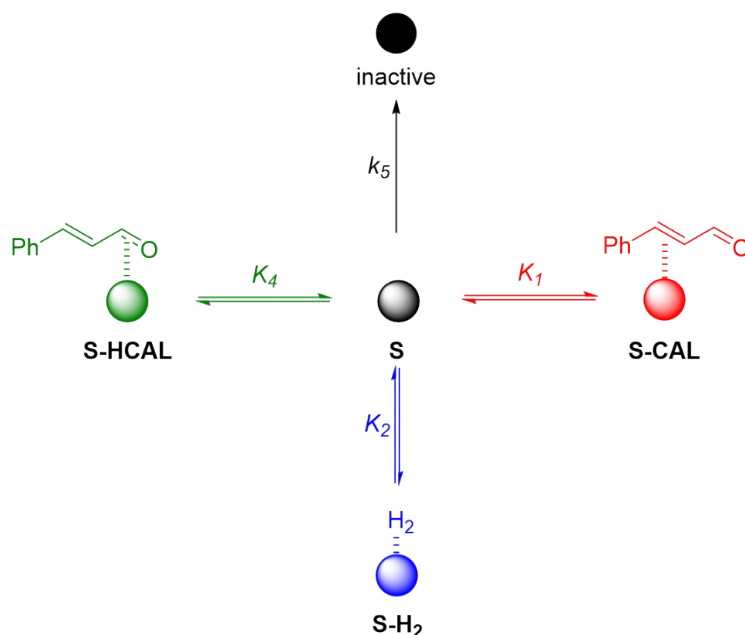
	Assumption	formula	
Rate	First order	$\dfrac{d[S_T]}{dt} = -k_5[S]$	(a)
S-CAL formation	Quasi equilibrium	$K_1 = \dfrac{[S-CAL]}{[S][CAL]}$	(b)
S-H$_2$ formation	Quasi equilibrium	$K_2 = \dfrac{[S-H_2]}{[S][H_2]}$	(c)
S-HCAL formation	Quasi equilibrium	$K_4 = \dfrac{[S-HCAL]}{[S][HCAL]}$	(d)
$[S_T]$		$[S_T] = [S] + [S-CAL] + [S-H_2] + [S-HCAL]$	(e)
(b), (c), (d) in (e)		$[S] = \dfrac{[S_T]}{(1 + K_1[CAL] + K_2[H_2] + K_4[HCAL])}$	(f)
(f) in (a)		$\dfrac{d[S_T]}{dt} = -k_5 \dfrac{[S_T]}{(1 + K_1[CAL] + K_2[H_2] + K_4[HCAL])}$	(g)
integration		$\dfrac{d[S_T]}{[S_T]} = -k_5 \dfrac{dt}{(1 + K_1[CAL] + K_2[H_2] + K_4[HCAL])}$	(h)
		$[S_T]_t = [S_T]_0 \exp(\dfrac{-k_5 t}{(1 + K_1[CAL] + K_2[H_2] + K_4[HCAL])}$	(1)

Figure S8. Depiction of the catalyst deactivation and the derivation of rate law describing the concentration of active sites $[S_T]$ at the time *t*, respectively τ with the corresponding assumptions.

Ph—CHO + ⬤ ⇌ (K₁) Ph—CHO (on sphere)

CAL   **S**   **S-CAL**

K_1

H₂ + ⬤ ⇌ (K₂) ⬤⋯H₂

S   **S-H₂**

K_2

⬤⋯H₂ + Ph—CHO(on sphere) → (k₃) ⬤ + Ph—CHO(on sphere)

S-H₂   **S-CAL**   **S**   **S-HCAL**

k_3

Ph—CHO(on sphere) ⇌ (K₂) ⬤ + Ph—CHO

S-HCAL   **S**   **HCAL**

K_2

	Assumption	formula	
Rate		$\dfrac{d[\mathrm{HCAL}]}{dt} = k_3[S-H_2][S-\mathrm{CAL}]$	(a)
S-CAL formation	Quasi equilibrium	$K_1 = \dfrac{[S-CAL]}{[S][CAL]}$	(b)
S-H₂ formation	Quasi equilibrium	$K_2 = \dfrac{[S-H_2]}{[S][H_2]}$	(c)
S-HCAL formation	Quasi equilibrium	$K_4 = \dfrac{[S-HCAL]}{[S][HCAL]}$	(d)
(b), (c) in (a)		$\dfrac{d[\mathrm{HCAL}]}{dt} = k_3 K_1 K_2 [H_2][\mathrm{CAL}][S]^2$	(e)
$[S_T]$		$[S_T] = [S] + [S-CAL] + [S-H_2] + [S-HCAL]$	(f)
(b), (c), (d) in (e)		$[S] = \dfrac{[S_T]}{(1 + K_1[CAL] + K_2[H_2] + K_4[HCAL])}$	(g)
(f) in (e)		$\dfrac{d[\mathrm{HCAL}]}{dt} = \dfrac{k_3 K_1 K_2 [H_2][\mathrm{CAL}][S_T]^2}{(1 + K_1[CAL] + K_2[H_2] + K_4[HCAL])^2}$	(2)

Figure S9. Derivation of the rate law for the Langmuir-Hinshelwood mechanism.

Determination of K_1, K_p and K_4

Assumption: The concentration of active sites $[S_T]$ does not change significantly during the initial stages of the reaction. Consequently, the amount of catalyst in solution is only dependent on the incubation period τ.

Deriving the corresponding equation to determine k_5:

(1) in (2)

$$\frac{d[HCAL]}{dt} = \frac{k_3 K_1 K_2 [H_2][CAL][S_T]_\tau^2}{(1 + K_1[CAL] + K_2[H_2] + K_4[HCAL])^2}$$ (3)

where

$$[S_T]_\tau = [S_T]_0 exp(-k_5\tau)$$ (4)

therefore

$$\ln\left(\frac{d[HCAL]}{dt}\right) = -2k_5\tau + \ln(a)$$ (5)

where

$$a = \frac{k_3 K_1 K_2 [H_2][CAL][S_T]_0^2}{(1 + K_1[CAL] + K_2[H_2] + K_4[HCAL])^2}$$ (6)

On a plot of $\ln\left(\frac{d[HCAL]}{dt}\right)$ vs. τ k_5 can be determined because here the slope is $slope = -2k_5$.

Analog K_1, K_p and K_4 can be determined. Here the example of K_1 will be discussed. The addition of cinnamaldehyde will change the equation 5 giving equation 7:

$$\ln\left(\frac{d[HCAL]}{dt}\right) = \frac{-2k_5\tau}{(1 + K_1[CAL]_\tau)} + \ln(a)$$ (7)

therefore

$$k_5^{-1}\ln\left(\frac{d[HCAL]}{dt}\right) = \frac{-2\tau}{(1 + K_1[CAL]_\tau)} + \ln(a)$$ (8)

According to equation 8 a plot of $k_5^{-1}\ln\left(\frac{d[HCAL]}{dt}\right)$ vs τ will produce a linear relationship where the slope is defined as $\frac{-2}{(1 + K_1[CAL]_\tau)}$, where $[CAL]_\tau$ being the concentration of CAL during the incubation period.

Table S2. Slopes found for the assessment of parameters influencing the catalyst deactivation.

Entry	Added reagent	Equation	slope	Value Pd	Value Pd$_{0.5}$Au$_{0.5}$
1	-	7	$-2k_5$	-0.66 h^{-1}	-0.26 h^{-1}
2	0.5 M CAL	8	$\frac{-2}{(1 + K_1[CAL]_\tau)}$	-0.57	-0.93

3	5 bar H_2	8	$\dfrac{-2}{(1 + K_p P(H_2))}$	-0.42	-0.19
4	0.5 M HCAL	8	$\dfrac{-2}{(1 + K_4[HCAL]_\tau)}$	-1.32	-0.09

Estimation of active sites after incubation time τ

Assuming that the initial rates are not affected by further catalyst deactivation and noticing that the reaction conditions are not altered to the reaction conditions to τ=0, one can articulate that the rate after the time τ is determined according to equation 9.

$$rate = \frac{d[HCAL]}{dt} = \frac{k_3 K_p K_1[CAL]P(H_2)[S_T]_\tau^2}{\left(1 + K_1[CAL] + K_p P(H_2) + K_4[HCAL]\right)^2} \tag{9}$$

The fraction of active sites can be estimated according to the following equations, assuming that $[S_T]_0$ is one (i.e. no catalyst deactivation takes place during the reaction set up).

$$\frac{rate_\tau}{rate_{\tau=0}} = \frac{\dfrac{k_3 K_p K_1[CAL]P(H_2)[S_T]_\tau^2}{\left(1 + K_1[CAL] + K_p P(H_2) + K_4[HCAL]\right)^2}}{\dfrac{k_3 K_p K_1[CAL]P(H_2)[S_T]_0^2}{\left(1 + K_1[CAL] + K_p P(H_2) + K_4[HCAL]\right)^2}} \tag{10}$$

$$\frac{rate_\tau}{rate_{\tau=0}} = \frac{[S_T]_\tau^2}{[S_T]_0^2} \tag{11}$$

$$\frac{[S_T]_\tau}{[S_T]_0} = \frac{\sqrt{rate_\tau}}{\sqrt{rate_0}} \tag{12}$$
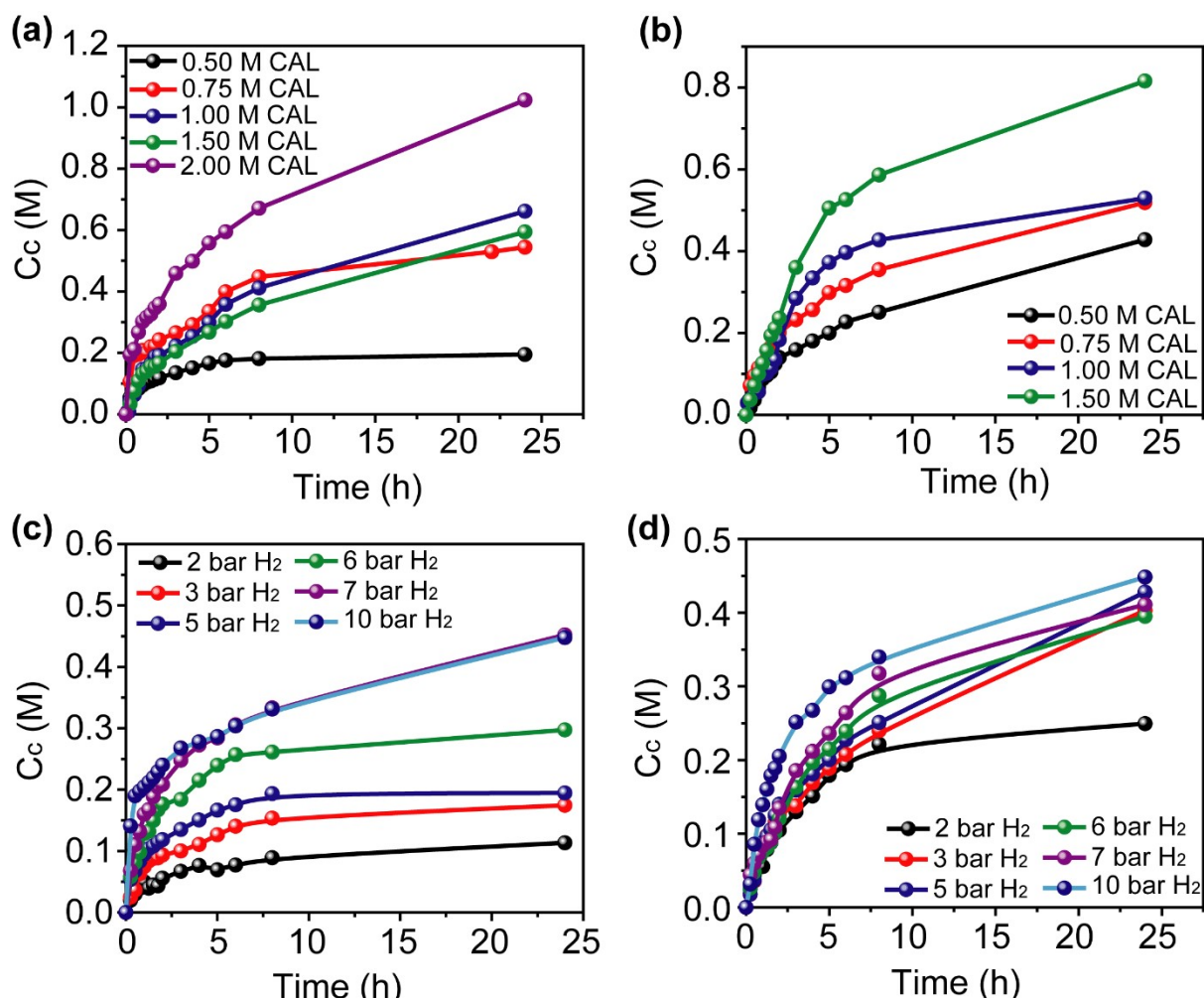
Different excess experiments

Figure S10. Kinetic traces found for Pd NPs ((**A**) and (**C**)) and $Pd_{0.5}Au_{0.5}$ NPs ((**B**) and (**D**)) under the variation of CAL ((**A**) & (**B**)) and $P(H_2)$ ((**C**) & (**D**)). Reaction conditions if not stated elsewise: THF (10 mL), T = 50°C, P (H_2) =5 bar, [CAL] = 0.5 M, catalyst (0.11 mg), [C_4C_1Im][NTf_2] (140 mg).

To evaluate the rate orders in the reaction, different excess experiments using CAL and H_2 were carried out.[7] Indeed, increasing both H_2 pressure and CAL concentration led to enhanced reaction rates, and thus higher conversions were obtained for Pd and $Pd_{0.5}Au_{0.5}$ NPs at 24 h of reaction (**Figure S9**). To quantify the rate orders for both reagents and product, and thus detail their effect in the overall reaction, a variable time normalized analysis (VTNA) was undertaken (**Figure S10**).[8-10]
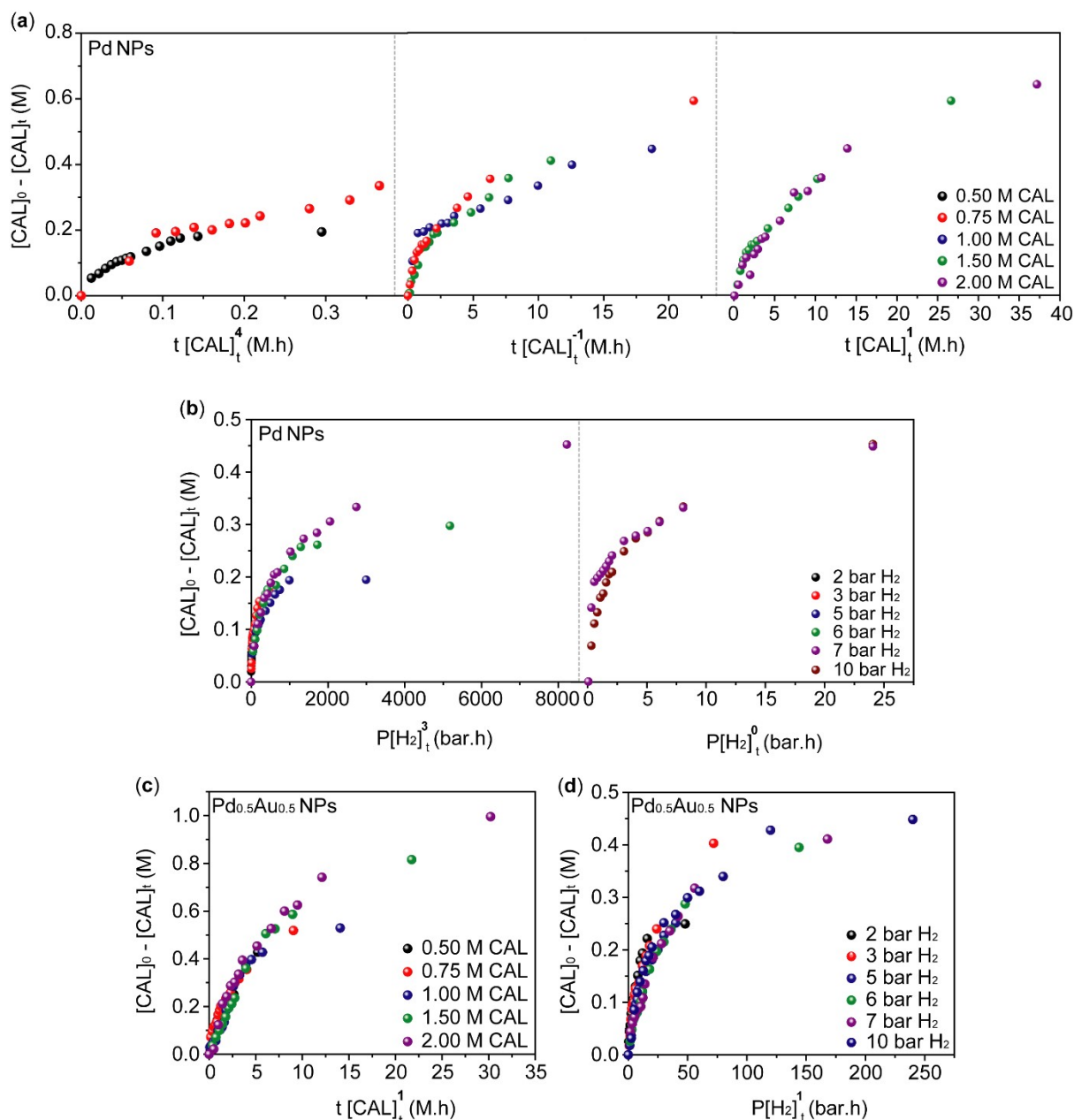
Figure S11. Determination of reagent orders for monometallic Pd and bimetallic $Pd_{0.5}Au_{0.5}$ NPs. (**a**) & (**b**) Variable time normalisation analysis (VTNA) undertaken with Pd and (**c**) & (**d**) VTNA for $Pd_{0.5}Au_{0.5}$NPs. (**a**) Time normalised analysis of kinetic traces obtained for Pd under the variation of CAL and constant H_2 pressure (5 bar). (**b**) Time normalised analysis obtained for Pd NPs under constant CAL concentration (0.5 M) whilst alternating the H_2 pressure. (**c**) Variable time normalisation analysis (VTNA) undertaken with $Pd_{0.5}Au_{0.5}$ NPs under the variation of CAL. (**d**) Time normalised analysis obtained for $Pd_{0.5}Au_{0.5}$ NPs under constant CAL concentration (0.5 M) whilst alternating the H_2 pressure. Standard reaction conditions for all presented data are if not investigated in the corresponding figure: THF (10 mL), T = 50°C, $P(H_2)$ = 5 bar, [CAL] =0.5 M, Pd concentration for both $Pd_{0.5}Au_{0.5}$ and Pd NPs as catalyst was 0.11 mg, and 130 mg $[C_4C_1Im][NTf_2]$. All kinetic traces depicted here are displayed as the consumed concentration of CAL, which equals the concentration of HCAL, see SI for further information (Note also under the essayed reaction conditions selectivity > 95%).

For Pd NPs, a reasonable visual overlay of the kinetic traces, and thus CAL and H_2 rate orders could not be found (**Figure S8a and b**). For example, upon varying the initial concentration of CAL, Pd NPs displayed three differing responses. At the concentration range of 0.5 M to 0.75 M an unexpected order > 1 for CAL was observed (**Figure S9**). This was associated to an increase of the catalyst stability at higher concentrations of CAL (**Figure 5 and Table 1**), and thus the overall beneficial effect of increased concentrations of reagents on the catalyst surface (**Figure S9**). In the range of 0.75 M to 1.5 M a competitive adsorption of CAL and H_2 on the active sites dominated the overall reaction rate (**Figure S9**), thus an order of *ca.* -1 is found (**Figure S8a**). At very high concentrations of CAL (>1.5 M) the stability of the catalyst was outweighing all other effects (**Figure S9**), including reactant inhibition, leading to an order 1 (**Figure S8d**). Similarly, the stability of Pd NPs seemed to increase with the H_2 pressure, which in turn influenced the overall rate of reaction (**Figure S9**), and thus an order >1 was found in the 2–7 bar H_2 pressure range. For higher H_2 pressure (up to 10 bar) no influence on the catalyst and reaction rates was observed (**Figure S8b and Figure S9**).

For $Pd_{0.5}Au_{0.5}$ NPs, a good visual overlay of kinetic traces was found for CAL and H_2, which were normalised to an order of 1 (**Figure S8c and S8d, Figure S9**), suggesting that neither CAL nor H_2 significantly poisoned the active sites of $Pd_{0.5}Au_{0.5}$ NPs. Additionally, these results confirmed the higher stability of $Pd_{0.5}Au_{0.5}$ NPs under the reaction conditions compared to Pd NPs, as a good overlay of the kinetic data can only be achieved for a relatively slow catalyst deactivation.
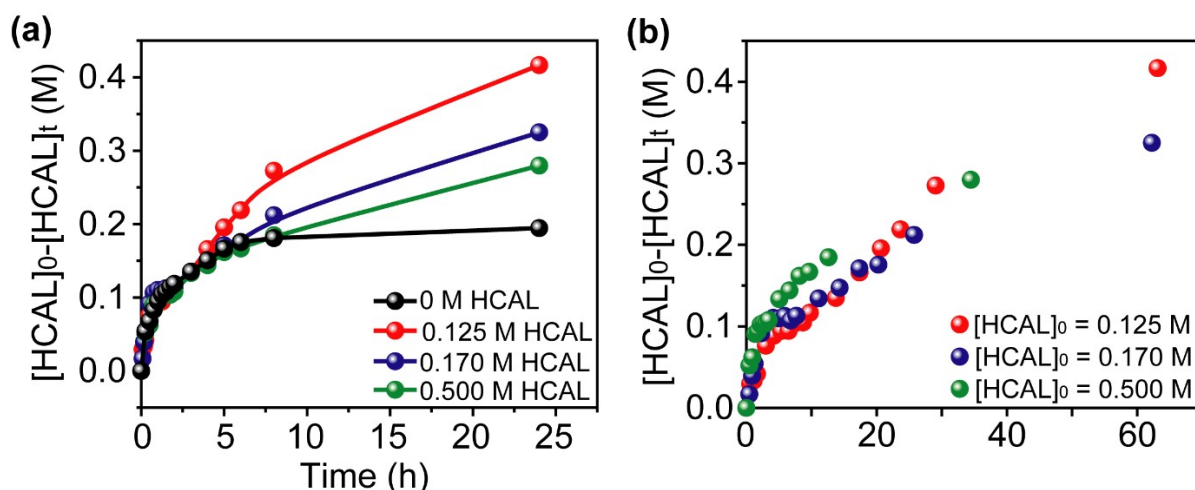
Figure S12. Different excess experiments with Pd with varying HCAL concentrations. (a) Initial HCAL addition in the range of 0 M to 0.5 M HCAL, and (b) VTNA analysis of the kinetic traces for initial addition of 0.125 M HCAL to 0.5 M HCAL. Reaction conditions: THF (10 mL), T = 50°C, $P(H_2)$ = 5 bar, [CAL] = 0.5 M, Pd NPs as catalyst was 0.11 mg, and 130 mg $[C_4C_1Im][NTf_2]$.
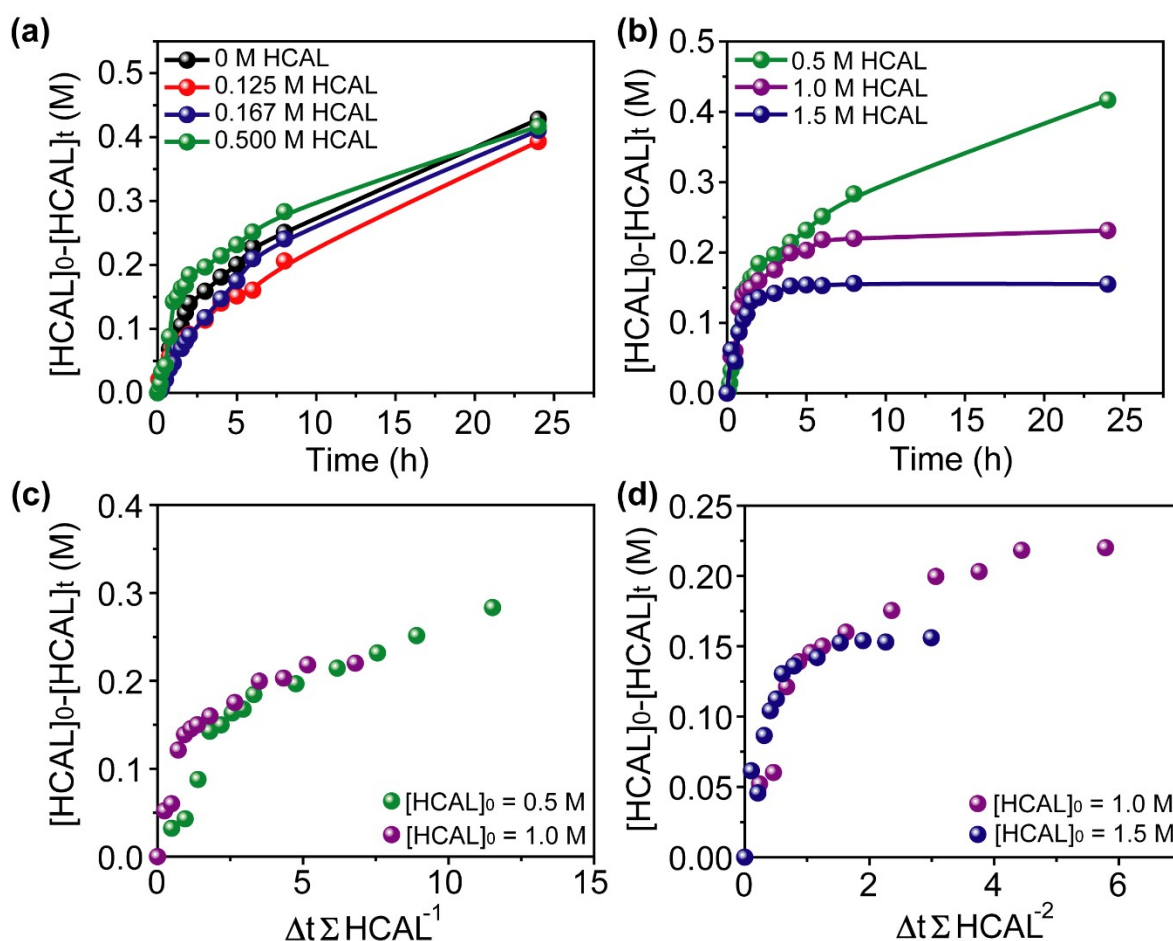

Figure S13. Different excess experiments with $Pd_{0.5}Au_{0.5}$ with varying HCAL concentrations. (a) Initial HCAL addition in the range of 0 M to 0.5 M HCAL, and (b) 0.5 M HCAL to 1.5 M HCAL. (c) VTNA analysis of the kinetic traces for initial addition of 0.5 M HCAL and 1.0 M HCAL, and (d) 1.0 M HCAL and 1.5 M HCAL. Reaction conditions: THF (10 mL), T = 50°C, $P(H_2)$ = 5 bar, [CAL] = 0.5 M, $Pd_{0.5}Au_{0.5}$ NPs as catalyst was 0.11 mg, and 130 mg $[C_4C_1Im][NTf_2]$.

<u>Estimation of the reduction of active sites during the selective hydrogenation of cinnamaldehyde</u>

The concentration of active sites at the time measurement t_i was estimated according to equation 9 (for visualising the equation is repeated below).

$$[S_T]_i = [S_T]_{i-1} exp(\frac{-k_5(t_i - t_{i-1})}{(1 + K_1(\frac{[CAL]_i - [CAL]_{i-1}}{2})^n + K_p P(H_2)^1 + K_4(\frac{[HCAL]_i - [HCAL]_{i-1}}{2})^{-1}}$$

Note that the descriptor i denotes for an individual measurement point. Furthermore, n was assumed to be 1 for $Pd_{0.5}Au_{0.5}$ NP, whilst for Pd NP a change from 1 to -1 was assumed at [CAL] >0.7M. The overall time normalisation presented in **Figure 5** is undertaken as described in the literature.[11]

<u>Turnover frequency (TOF) calculations for surface sites</u>

The volume of one Pd(Au) nanoparticle can be calculated according to $V_{Pd} = \frac{1}{6}\pi d^3 = 4.1 \cdot 10^{-27} m^3$ and $V_{Au} = \frac{1}{6}\pi d^3 = 1.2 \cdot 10^{-26} m^3$.

The occupied volume is calculated by multiplying these values by 0.75. The volume of one Pd(Au) atom are tabulated as $2.7 \cdot 10^{-30} m^3 (3.3 \cdot 10^{-30} m^3)$. Dividing the occupied volume by the volume of one atom gives the total amount of Pd(Au) atoms in one particle: Atoms Pd_{NP} = 1117 and Atoms Au_{NP} = 2723.

The volume of the subsurface can be calculated by subtracting two times the diameter of one atom of Pd(Au) from the total diameter of the NP. Thereafter, the atoms in the subsurface can be calculated. Dividing the surface atoms by the total amount of atoms in one nanoparticle the dispersion can be calculated. For the bimetallic catalysts, a linear relationship between the Pd/Au ratio and surface sites is assumed. We found the following values for the surface sites ratio and amount after accounting for the varying metal concentrations:

Table S3. Calculated metal content in the reaction mixture, surface sites ratio, concentration of surface sites and TOF.

Entry	Catalyst	Total metal content in reaction mixture/ mmol	Surface sites ratio	$C_{surface\ sites}$/ M	TOF/ h^{-1}
1	Pd	0.005	0.36	0.00018	83
2	$Pd_{0.75}Au_{0.25}$	0.00625	0.34	0.00021	329
3	$Pd_{0.5}Au_{0.5}$	0.00875	0.32	0.00028	82
4	$Pd_{0.25}Au_{0.75}$	0.0125	0.30	0.00038	10
5	Au	0.005	0.28	0.00014	0

5. Theoretical calculations

Density functional theory (DFT) computations were performed using Gaussian 16 Revision A.03. [12] The PBE0 hybrid exchange-correlation functional[13] was employed with the Def2-SVP basis set[14] to describe H, C and O atoms, and the Def2-SV(P) basis set[14] to describe Pd atoms. The Def2-SV(P) basis set features an effective core potential (ECP)[15] to describe 28-core electrons on Pd, [Ar] $3d^{10}$.

Pd is in it zero oxidation state and the total charge is zero. All clusters are in high-spin configurations with a multiplicity of 9. Initial geometries for Pd_{19} and Pd_{19}-$2H_2$ (with one H_2 removed) are from the study of Pelzer et al.[16] Geometry optimisation followed by analytic harmonic vibrational frequency calculation was carried out for all species for thermochemical corrections at 298.15 K and 1 atm.

Figure S13 displays optimised structures for adsorption of H_2 and CAL onto Pd_{19}.
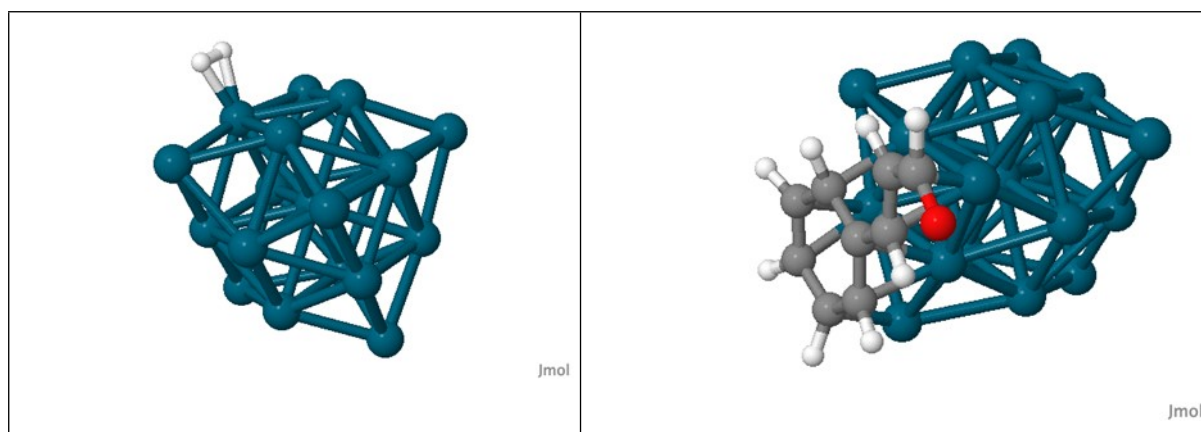
(a)	(b)

Figure S14. DFT optimised structures for (a) H_2 and (b) CAL adsorption onto the Pd_{19} cluster.

6. References

1.   Huddleston, J. G.; Visser, A. E.; Reichert, W. M.; Willauer, H. D.; Broker, G. A.; Rogers, R. D., Characterization and comparison of hydrophilic and hydrophobic room temperature ionic liquids incorporating the imidazolium cation. *Green Chemistry* **2001,** *3* (4), 156-164.

2.   Bonhôte, P.; Dias, A.-P.; Papageorgiou, N.; Kalyanasundaram, K.; Grätzel, M., Hydrophobic, Highly Conductive Ambient-Temperature Molten Salts. *Inorganic Chemistry* **1996,** *35* (5), 1168-1178.

3.   Santos, A. R.; Blundell, R. K.; Licence, P., XPS of guanidinium ionic liquids: a comparison of charge distribution in nitrogenous cations. *Physical Chemistry Chemical Physics* **2015,** *17* (17), 11839-11847.

4.   Cano, I.; Weilhard, A.; Martin, C.; Pinto, J.; Lodge, R. W.; Santos, A. R.; Rance, G. A.; Åhlgren, E. H.; Jónsson, E.; Yuan, J.; Li, Z. Y.; Licence, P.; Khlobystov, A. N.; Alves Fernandes, J., Blurring the boundary between homogenous and heterogeneous catalysis using palladium nanoclusters with dynamic surfaces. *Nature Communications* **2021,** *12* (1), 4965.

5.   Sun, X.; Dawson, S. R.; Parmentier, T. E.; Malta, G.; Davies, T. E.; He, Q.; Lu, L.; Morgan, D. J.; Carthey, N.; Johnston, P.; Kondrat, S. A.; Freakley, S. J.; Kiely, C. J.; Hutchings, G. J., Facile synthesis of precious-metal single-site catalysts using organic solvents. *Nature Chemistry* **2020,** *12* (6), 560-567.

6.   Kohlrausch, E. C.; Centurion, H. A.; Lodge, R. W.; Luo, X.; Slater, T.; Santos, M. J. L.; Ling, S.; Mastelaro, V. R.; Cliffe, M. J.; Goncalves, R. V.; Alves Fernandes, J., A high-throughput, solvent free method for dispersing metal atoms directly onto supports. *Journal of Materials Chemistry A* **2021,** *9* (47), 26676-26679.

7.   Luza, L.; Rambor, C. P.; Gual, A.; Alves Fernandes, J.; Eberhardt, D.; Dupont, J., Revealing Hydrogenation Reaction Pathways on Naked Gold Nanoparticles. *ACS Catalysis* **2017,** *7* (4), 2791-2799.

8.   Nielsen, C. D. T.; Burés, J., Visual kinetic analysis. *Chemical Science* **2019,** *10* (2), 348-353.

9.   Burés, J., Variable Time Normalization Analysis: General Graphical Elucidation of Reaction Orders from Concentration Profiles. *Angewandte Chemie International Edition* **2016,** *55* (52), 16084-16087.

10.   Burés, J., A Simple Graphical Method to Determine the Order in Catalyst. *Angewandte Chemie International Edition* **2016,** *55* (6), 2028-2031.

11.   Martínez-Carrión, A.; Howlett, M. G.; Alamillo-Ferrer, C.; Clayton, A. D.; Bourne, R. A.; Codina, A.; Vidal-Ferran, A.; Adams, R. W.; Burés, J., Kinetic Treatments for Catalyst Activation and Deactivation Processes based on Variable Time Normalization Analysis. *Angewandte Chemie International Edition* **2019,** *58* (30), 10189-10193.

12.   Frisch, M. J.; Trucks, G. W.; Schlegel, H. B.; Scuseria, G. E.; Robb, M. A.; Cheeseman, J. R.; Scalmani, G.; Barone, V.; Petersson, G. A.; Nakatsuji, H.; Li, X.; Caricato, M.; Marenich, A. V.; Bloino,

J.; Janesko, B. G.; Gomperts, R.; Mennucci, B.; Hratchian, H. P.; Ortiz, J. V.; Izmaylov, A. F.; Sonnenberg, J. L.; Williams; Ding, F.; Lipparini, F.; Egidi, F.; Goings, J.; Peng, B.; Petrone, A.; Henderson, T.; Ranasinghe, D.; Zakrzewski, V. G.; Gao, J.; Rega, N.; Zheng, G.; Liang, W.; Hada, M.; Ehara, M.; Toyota, K.; Fukuda, R.; Hasegawa, J.; Ishida, M.; Nakajima, T.; Honda, Y.; Kitao, O.; Nakai, H.; Vreven, T.; Throssell, K.; Montgomery Jr., J. A.; Peralta, J. E.; Ogliaro, F.; Bearpark, M. J.; Heyd, J. J.; Brothers, E. N.; Kudin, K. N.; Staroverov, V. N.; Keith, T. A.; Kobayashi, R.; Normand, J.; Raghavachari, K.; Rendell, A. P.; Burant, J. C.; Iyengar, S. S.; Tomasi, J.; Cossi, M.; Millam, J. M.; Klene, M.; Adamo, C.; Cammi, R.; Ochterski, J. W.; Martin, R. L.; Morokuma, K.; Farkas, O.; Foresman, J. B.; Fox, D. J. *Gaussian 16 Rev. C.01*, Wallingford, CT, 2016.

13.   Adamo, C.; Barone, V., Toward reliable density functional methods without adjustable parameters: The PBE0 model. *The Journal of Chemical Physics* **1999,** *110* (13), 6158-6170.

14.   Weigend, F.; Ahlrichs, R., Balanced basis sets of split valence, triple zeta valence and quadruple zeta valence quality for H to Rn: Design and assessment of accuracy. *Physical Chemistry Chemical Physics* **2005,** *7* (18), 3297-3305.

15.   Andrae, D.; Häußermann, U.; Dolg, M.; Stoll, H.; Preuß, H., Energy-adjustedab initio pseudopotentials for the second and third row transition elements. *Theoretica chimica acta* **1990,** *77* (2), 123-141.

16.   Pelzer, A. W.; Jellinek, J.; Jackson, K. A., H2 Reactions on Palladium Clusters. *The Journal of Physical Chemistry A* **2013,** *117* (40), 10407-10415.